The FEBS Journal

FEBS PRESS science publishing by scientists

# Catalases of the polyextremophylic Andean isolate *Acinetobacter* sp. Ver 3 confer adaptive response to $H_2O_2$ and UV radiation

Mariana Gabriela Sartorio, Guillermo Daniel Repizo and Néstor Cortez

Instituto de Biología Molecular y Celular de Rosario (UNR & CONICET), Facultad de Ciencias Bioquímicas y Farmacéuticas, Universidad Nacional de Rosario, Argentina

**Keywords**
*Acinetobacter*; Andean wetlands; catalase; oxidative stress; UV radiation

**Correspondence**
G. D. Repizo, Facultad de Ciencias Bioquímicas y Farmacéuticas, Instituto de Biología Molecular y Celular de Rosario (UNR & CONICET), Universidad Nacional de Rosario, Suipacha 531, Rosario S2002LRK, Argentina
Tel: +54 341 435 0596/435 0661/435 1235 ext 140
E-mails: repizo@ibr-conicet.gov.ar

Deceased on 17 October 2019

(Received 15 June 2019, revised 18 November 2019, accepted 7 February 2020)

doi:10.1111/febs.15244

The polyextremophilic strain *Acinetobacter* sp. Ver3 isolated from high-altitude Andean lakes exhibits elevated tolerance to UV-B radiation and to pro-oxidants, a feature that has been correlated to its unusually high catalase activity. The Ver3 genome sequence analysis revealed the presence of two genes coding for monofunctional catalases: $^{AV3}$KatE1 and $^{AV3}$KatE2, the latter harboring an N-terminal signal peptide. We show herein that $^{AV3}$KatE1 displays one of the highest catalytic activities reported so far and is constitutively expressed at relatively high amounts in the cytosol, acting as the main protecting catalase against $H_2O_2$ and UV-B radiation. The second catalase, $^{AV3}$KatE2, is a periplasmic enzyme strongly induced by both peroxide and UV, conferring supplementary protection against pro-oxidants. The N-terminal signal present in $^{AV3}$KatE2 was required not only for transport to the periplasm via the twin-arginine translocation pathway, but also for proper folding and subsequent catalytic activity. The analysis of catalase distribution among 114 *Acinetobacter* complete genomes revealed a great variability in the catalase classes, with *A. baumannii* clinical isolates exhibiting higher numbers of isoenzymes and the most variable profiles.

## Introduction

High-altitude Andean lakes (HAAL), distributed along the central Andes area in South America, undergo extreme environmental conditions such as high concentrations of salt and metalloids, wide daily variations of temperature, and an elevated UV radiation [1]. These ecosystems thus became a good source of extremophile microorganisms displaying diverse biological strategies to cope with hostile environments. Indeed, about 1000 bacterial strains have been recently isolated from this area, embodying the Extremophile Culture Collection from HAAL [2,3].

*Acinetobacter* sp. Ver3 and Ver7, two phylogenetically related strains from the Verde lake located at 4400 m above sea level, were shown to display high tolerance to chemical pro-oxidants as $H_2O_2$ and methyl viologen (MV) when compared with collection strains of *A. baumannii*, *A. lwoffii*, and *A. johnsonii* used as controls [4]. Interestingly, the two strains also showed higher survival after UV-B radiation exposure, both in solid agar plates and in liquid cultures [4,5].

Measurements of photoproducts after exposure of *Acinetobacter* cultures to UV-B radiation and subsequent photoreactivation conditions provided evidence of the involvement of photolyases in an efficient DNA repairing pathway, possibly contributing to the observed resistant mechanisms to the harmful environment [5]. A PCR screening using degenerate primers on Ver3 DNA allowed identification of a gene with

**Abbreviations**
HAAL, high-altitude Andean lakes; HP, hydroperoxidase; MV, methyl viologen.

good homology to CPE-I type photolyases found in other *Acinetobacter* genomes. More recently, this photolyase from *Acinetobacter* sp. Ver3 was cloned and shown to prevent accumulation of photoproducts from damaged DNA after UV-B exposure of *Escherichia coli*-transformed cells [6].

The high tolerance toward pro-oxidants displayed by the Andean *Acinetobacter* isolates led to evaluation of their antioxidant enzymes. Both Ver3 and Ver7 isolates exhibited a single electrophoretic catalase species in soluble extracts and a total activity fifteen times higher than those found in collection strains *A. baumannii*, *A. johnsonii*, and *A. lwoffii* used as controls. Moreover, the presence of the catalase inhibitor 3-amino-triazole in the culture media reduced the observed tolerance to UV-B radiation, strongly suggesting the involvement of catalase activity in the biochemical mechanism of that response [4].

Catalases, peroxidases, and superoxide dismutases are the most important activities involved in the scavenging of reactive oxygen species (ROS) resulting from partial reduction of oxygen in aerobic cells. $H_2O_2$, the most abundant ROS, is formed as by-product of the respiratory electron transport chain through the two-electron reduction of molecular dioxygen or by disproportionation of the superoxide ion catalyzed by superoxide dismutases. Evolution led to appearance of three enzyme families that catalyze $H_2O_2$ dismutation, namely monofunctional heme catalases (hydroperoxidases II, HPII or KatEs), bifunctional heme catalases–peroxidases (hydroperoxidases I, HPI or KatGs), and nonheme Mn-catalases. More recently, phylogenetic studies revealed the existence of three clades for the typical monofunctional HPII: clade 1 of plant origin, clade 2 referred as 'large subunit' catalases of fungal–bacterial origin, and clade 3 including the 'small subunit' catalases present in bacteria and Archaea [7].

Efforts have been made to determine the participation of catalases from diverse *Acinetobacter* clinical isolates in the defense to ROS produced by neutrophils during infection, and also in the direct response to pro-oxidants *in vitro*. Recent studies on the Δ*katE* and Δ*katG* mutants of *A. baumannii* AB5075 and *A. nosocomialis* M2 indicated that the monofunctional catalase KatE accounts for the major part of the catalase activity displayed by the bacterium. However, the results also suggested that the bifunctional catalase–peroxidase KatG would be the activity responsible of tolerance to external peroxides *in vivo* [8].

Analysis of the complete genome of *Acinetobacter* sp. Ver3 revealed the presence of at least two genes encoding monofunctional heme catalases (EC 1.11.1.6), a cytosolic KatE (EZQ12194) and a periplasmic KatE (EZQ11977) carrying a putative translocation signal peptide [9]. A proteomic study reported in the same article showed a relative increase of the cytosolic catalase in cells cultured under UV-B, suggesting its involvement in the response to this radiation [9].

We describe herein the cloning of two genes encoding the catalases present in the polyextremophile *Acinetobacter* sp. Ver3, the localization and biochemical characterization of the protein products, and the first analysis of their involvement in the antioxidant protection of this bacterial strain. A phylogenetic analysis including 114 publicly available complete genomes of *Acinetobacter* strains was also performed in order to explore the diversity of catalase-encoding genes in this genus.

## Results

### Cloning, expression, and activity of *Acinetobacter* sp. Ver3 catalases

The complete genome sequence of the strain *Acinetobacter* sp. Ver3 has been reported, revealing the presence of two genes coding for heme catalases [9]. Sequence alignments indicate that the product of CL42_01515 (ORF EZQ12194) corresponds to a monofunctional heme catalase, classified as hydroperoxidase type II (HPII) or KatE, and related to the phylogenetically defined clade 3 [7,10], that will be named to as $^{AV3}$KatE1.

Using the primers detailed (Materials and methods, Table 1), the coding region of the gene CL42_01515 (1521bp) was amplified through PCR protocols from genomic DNA. The resulting *Nco*I–*Hind*III fragment was cloned in compatible sites of the pET28 expression vector, originating pEV3K1, and finally used to transform *E. coli* BL21 (DE3) cells. After induction with IPTG, transformed cells were subjected to sonic rupture, and recombinant catalase was purified to homogeneity from soluble fractions using ammonium sulfate precipitation, dialysis, and anionic exchange chromatography as described below (Fig. 1A,B).

The purified enzyme displayed an absorbance spectrum typical of heme catalases [11,12] with the Soret band at 405 nm, and the Q bands at 515, 540, 575, and 630 nm (Fig. 1D).

The enzymatic activity of recombinant $^{AV3}$KatE1 was monitored by following the decomposition of $H_2O_2$, which allowed estimation of a $k_{cat}$ of $1.3 \pm 0.2.10^7$ $s^{-1}$ and a $K_m = 229 \pm 56$ mM, that result in one of the highest catalytic activities reported so far for this type of enzymes. Comparison of the electrophoretic mobility after nondenaturing PAGE

**Table 1.** List of primers. The underlined sequences correspond to restriction enzymes recognition sites: [a] *Nco*I, [b] *Hind*III, [c] *Nde*I.

| Primers | Sequence (5′–3′) |
|---|---|
| KatE1F | 5′-TGACCATGGGCGATGACTCAA-3′[a] |
| KatE1upF | 5′-CGTAAGCTTTACTGTAAATCATCGTTA-3′[b] |
| KatE1R | 5′-CAGAAGCTTTTATTGTATTCGGGAAG-3′[b] |
| KatE2F | 5′-AACCATATGTTTAAGCGTTCAATG-3′[c] |
| KatE2upF | 5′-CATAAGCTTCACCATCCACAACGA-3′[b] |
| KatE2matF | 5′-TCACATATGCCATTAACAAAAGATAACG-3′[c] |
| KatE2R | 5′-GGCAAGCTTTTGAGTTTTACAGGA-3′[b] |
| M13F | 5′-GTAAAACGACGGCCAGT-3′ |
| M13R | 5′-GGAAACAGCTATGACCATG-3′ |
| KatEADPF | 5′-TGTCATCATGCGACTTATCCATGG-3′ |
| KatEADPR | 5′-CAACGAACCATGGCAATTCATTATCG-3′ |
| qkatE1F | 5′-ATTGAACGTGGTGATTTCCCG-3′ |
| qkatE1R | 5′-GGCAGCTTGTTCTACGTCTTG-3′ |
| qkatE2F | 5′-GTTCCCAGACTTCATCCACG-3′ |
| qkatE2R | 5′-ACCGAAACCGTCTTGTTCAC-3′ |
| qrecAF | 5′-CTCAATATGCTCGCAAACTTGG-3′ |
| qrecAR | 5′-GGTTAAGGCTGCTACAGAATCG-3′ |
| qrpoBF | 5′-TGCAAACACGGTTCTTAGCC-3′ |
| qrpoBR | 5′-CACCTGGACGCATTACCTTG-3′ |

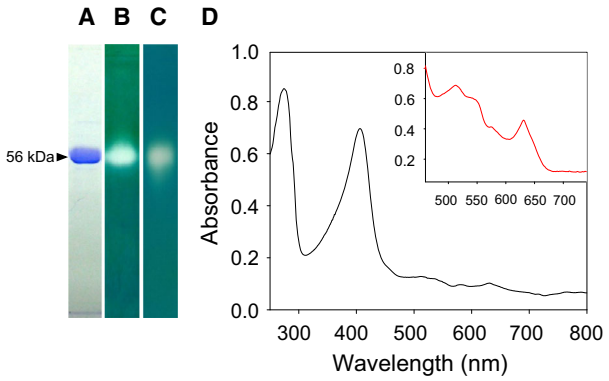


**Fig. 1.** Purification of $^{AV3}$KatE1. (A) Coomassie blue staining of purified KatE1 after SDS/PAGE; (B) *in situ* catalase activity staining of purified $^{AV3}$KatE1 after nondenaturating PAGE; (C) *in situ* catalase activity staining of *Acinetobacter* Ver3 total soluble extracts after nondenaturating PAGE (D) Absorption spectrum of purified $^{AV3}$KatE1 (0.4 mg·mL$^{-1}$) showing the Soret band at 405 nm. Details of Q bands obtained with concentrated protein (4 mg·mL$^{-1}$) are visible in the inset (red). Data shown are representative of three independent experiments.

showed that recombinant $^{AV3}$KatE1 corresponds to the single activity species observed in soluble extracts of *Acinetobacter* sp. Ver3.

The product of the second heme catalase gene CL42_02730 (ORF EZQ11977) also displayed homology with HPII/KatE catalases, structurally related to clade 1 [10], and was accordingly denominated $^{AV3}$KatE2. Different export-sequence prediction softwares identified the presence of a 19-residue signal peptide with cleavage site encoded by the gene [9], suggesting a periplasmic localization for $^{AV3}$KatE2 catalase.

Two sequences were amplified by PCR using genomic Ver3 DNA as template and the primers detailed in Table 1: the complete *katE2* gene ($^{AV3}$*katE2*) and the same sequence lacking the signal peptide coding region ($^{AV3}$*katE2*$^{-P}$). Both amplified sequences were cloned in *Nde*I-*Hind*III compatible sites of pET22 plasmid, originating pEV3K2 and pEV3K2$^{-P}$, respectively. However, *E. coli* BL21 (DE3) cells transformed with any of these two vectors did not accumulate protein products after induction with IPTG (not shown). In a different attempt to obtain the recombinant enzyme, we cotransformed BL21 (DE3) cells with the pKJE7 plasmid harboring *dnaK*, *dnaJ*, and *grpE* chaperone genes (Takara Bio USA Inc., St. Louis, MO, USA) and each of the aforementioned pET22 derivative vectors (Table 2). Induction with IPTG and L-arabinose promoted accumulation of *Acinetobacter* Ver3 recombinant catalases, which were visualized after protein staining of SDS/PAGE. Isolation of the recombinant enzymes from soluble extracts was achieved after ammonium sulfate precipitation followed by anionic interchange chromatography (Fig. 2A).

Soluble extracts from induced pEV3K2- or pEV3K2$^{-P}$-transformed cells showed spectral differences. While the full gene promotes expression of an active enzyme with a Soret band at 410 nm, the *katE2*$^{-P}$ gene encodes an inactive enzyme displaying a 5 nm blueshift. This suggests an altered environment of the heme moiety, probably following an irregular folding (Fig. 2B).

Recombinant active $^{AV3}$KatE2 was purified to homogeneity using ammonium sulfate precipitation, dialysis, and anionic chromatography (Fig. 2, lane 5). Kinetic parameters of the purified enzyme were estimated, resulting in a $k_{cat} = 2.14 \pm 0.3.10^5$ s$^{-1}$ and a $K_m = 6.5 \pm 0.6$ mM.

## While $^{AV3}$KatE1 is strictly cytosolic, $^{AV3}$KatE2 can be directed to the periplasm

To determine the localization of the recombinant Ver3 catalases, *E. coli* BL21 (DE3) cells were cotransformed with pKJE7 and either pEV3K1 or pEV3K2. Subsequent cellular fractionation was carried out after IPTG and arabinose treatment to induce the exogenous genes. Bacteria were lysed in isotonic buffer, and subcellular fractions were obtained as described in Materials and methods.

**Table 2.** List of strains and plasmids used in this work.

| | Description | Reference |
|---|---|---|
| Strains | | |
| *Acinetobacter* | | |
| *A.* sp. Ver3 | | [2] |
| *A. baylyi* ADP1 | | DSMZ |
| *A. baylyi* ADP1 *kat*$^-$ | ADP1; *katE*::Km | This work |
| *E. coli* | | |
| DH5α | Φ80 *lac*ZDM15 *rea*A1 *end*A1 *gyr*A96 *thi*-1 *hsd*R17 *sup*E44 *rel*A1 *deo*R D(*lac*ZYA-*arg*F) U169 F | [40] |
| BL21 (DE3) | F$^-$ *ompT* ($r_B^-$ $m_B^-$) *gal dcm* λ(DE3) | [41] |
| MC4100 | F$^-$ *araD139 Δ*(*argF-lac*) *U169 rpsL150 relA1 deoC1 ptsF25 rpsR flbB301* | [42] |
| CU165 | MC4100; *zhd33*::Tn*10 secY40* (Tc$^r$) | [43] |
| B1LK0 | MC4100; Δ*tatC* | [44] |
| Plasmids | | |
| pKJE7 | DnaK, DnaJ GrpE chaperone expression, $Cm^R$ | Takara® |
| pET28 | Expression vector, $Km^R$ | Novagen® |
| pET22 | Expression vector, $Ap^R$ | Novagen® |
| pEV3K1 | pET28 derivative expressing $^{AV3}$*katE1* | This work |
| pEV3K2 | pET22 derivative expressing $^{AV3}$*katE2* | This work |
| pEV3K2$^{-p}$ | pET22 derivative expressing $^{AV3}$*katE2* without the sequence codifying the signal peptide | This work |
| pUC4K | Vector containing Kanamycin cassette ($Km^R$, $Ap^R$) | [45] |
| pGEM®T-Easy | Cloning vector | Promega® |
| pGAK1 | pGEM®T-Easy derivative containing 2332-bp fragment corresponding to ADP1 *katE* gene | This work |
| pGAK1km | pGAK1::Km at EcoRV site | This work |
| pMBLe(OA) | Expression vector pMBLe derivative; contains origin of replication from pWH1277 at *Age*I site, $Gm^R$ | [46] |
| pMV3K1 | pMBLe(OA) derivative expressing $^{AV3}$*katE1* | This work |
| pMV3K2 | pMBLe(OA) derivative expressing $^{AV3}$*katE2* | This work |

Cells transformed with pEV3K1 showed an induced protein band of 58 kDa only in the cytosolic fraction (Fig. 3A, lane 3), while the pEV3K2 transformants contained a 54-kDa protein corresponding to the $^{AV3}$KatE2 in both cytosolic and periplasmic fractions (Fig. 3A, lanes 5 and 6), as it was observed by SDS/PAGE. The only periplasmic extract exhibiting catalase activity corresponded to the cells expressing the $^{AV3}$*katE2* complete gene (Fig. 3B). Moreover, cells expressing the $^{AV3}$*katE2*$^{-P}$ lacking the signal peptide were less efficient in translocating the protein to periplasm, as it was confirmed using specific anti-KatE2 antibodies (Fig. 3C).

Two major secretion routes for translocation of proteins to the periplasm have been described in bacteria: the general secretion pathway (Sec) and the twin-arginine translocation pathway (TAT). To identify the machinery utilized for KatE2 translocation, *E. coli* MC4100 mutants in Sec or TAT proteins were cotransformed with pEV3K2 and pKJE7. After induction, *wt* cells were able to accumulate KatE2 protein in the periplasm, as did the *secY*$^{ts}$ mutant (Fig. 4). On the contrary, the Δ*tat*C mutant failed to show protein accumulation in any fraction. Identity of the overexpressed bands was determined using anti-KatE2 antibodies (Fig. 4, lower panel).

## $^{AV3}$*katE2* expression increases after $H_2O_2$ and UV treatments

Expression of the $^{AV3}$*katE1* and $^{AV3}$*katE2* genes was studied in *Acinetobacter Ver3* cells subjected to pro-oxidant challenges. Cultures in exponential growth phase were exposed to $H_2O_2$ (1 mM) or UV-B radiation (900 J·m$^{-2}$), and immunostaining of total soluble extracts was carried out after SDS/PAGE using polyclonal antibodies. Exposure to $H_2O_2$ or UV promotes accumulation of $^{AV3}$KatE2 but no visible enhancement of the $^{AV3}$KatE1 signal was observed (Fig. 5).

In order to determine whether there existed a correlation at the transcriptional level, total RNA was isolated at 10 and 30 min after exposure of the cells to $H_2O_2$ or UV radiation, and quantitative real-time reverse transcription PCR (qRT-PCR) was performed. Results illustrated in Fig. 5 show that $^{AV3}$*katE2* expression levels increased about 100- and 20-fold after only 10 min of $H_2O_2$ or UV challenge, respectively, whereas the $^{AV3}$*katE1* transcript did not exhibit significant variation (Fig. 5).

## $^{AV3}$KatE1 plays a critical protective role against pro-oxidant treatments

*Acinetobacter baylyi* ADP1 possesses only one cytosolic catalase (CAG67388.1) belonging to the phylogenetically defined clade 3 [7,10] that shares 89% protein sequence identity with $^{AV3}$KatE1.

In order to investigate the involvement of Ver3 catalases in the tolerance to UV radiation and pro-oxidant challenges, we constructed a catalase-deficient ADP1

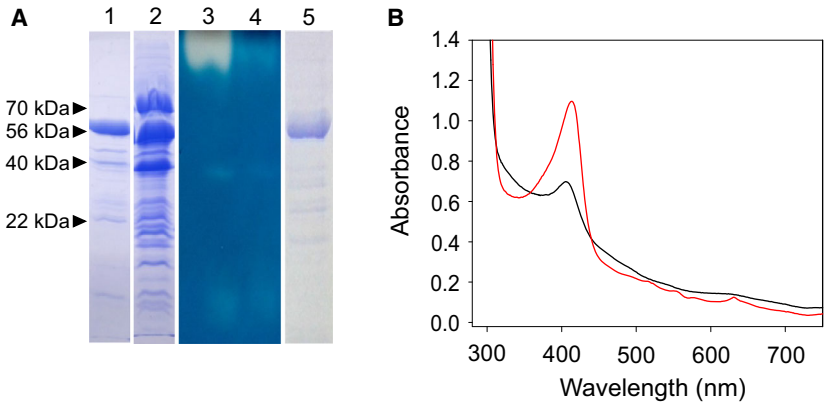


**Fig. 2.** Expression and isolation of $^{AV3}$KatE2. (A) Soluble extracts from cultured *Escherichia coli* BL21 (DE3)-transformed cells carrying the pEV3K2 or pEV3K2$^{-P}$ plasmids and the pKJE7. Lanes 1 and 2 show protein staining of SDS/PAGE from fractions obtained after ion-exchange chromatography of *E. coli* cells expressing $^{AV3}$*katE2* or $^{AV3}$*katE2*$^{-P}$, respectively. Lanes 3 and 4 correspond to *in situ* catalase activity after nondenaturing PAGE of soluble extracts from *E. coli* cells expressing $^{AV3}$*katE2* or $^{AV3}$*katE2*$^{-P}$, respectively. Lane 5 shows SDS/PAGE protein staining of purified KatE2 from pEV3K2 *E. coli*-transformed cells. (B) Spectra of extracts corresponding to recombinant catalase from pEV3K2 (black) or pEV3K2$^{-P}$ (red) transformants. Data displayed are representative of three independent experiments.

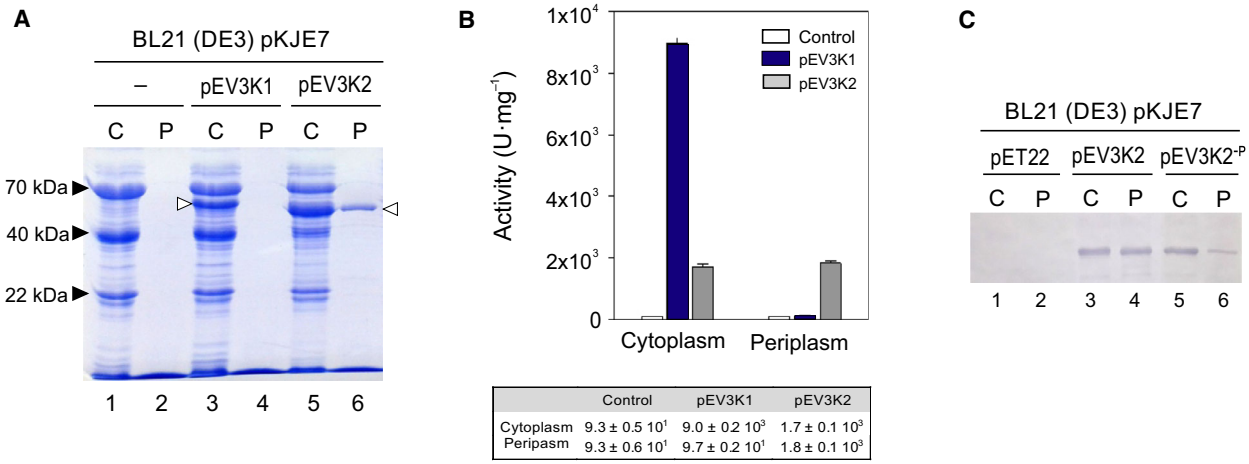


| | Control | pEV3K1 | pEV3K2 |
|---|---|---|---|
| Cytoplasm | 9.3 ± 0.5 $10^1$ | 9.0 ± 0.2 $10^3$ | 1.7 ± 0.1 $10^3$ |
| Peripasm | 9.3 ± 0.6 $10^1$ | 9.7 ± 0.2 $10^1$ | 1.8 ± 0.1 $10^3$ |

**Fig. 3.** Localization of $^{AV3}$KatE1 and $^{AV3}$KatE2. (A) Coomassie blue staining of SDS/PAGE from cytosolic-C- or periplasmic-P-soluble fractions (15 μL) from *Escherichia coli* cells carrying pKJE7 (lanes 1 and 2) cotransformed with pEV3K1 (lanes 3 and 4) or pEV3K2 (lanes 5 and 6). Black arrows indicate the expressed chaperones encoded in pKJE7 (70, 40, and 22 kDa); white arrows indicate expression of $^{AV3}$KatE1 (lane 3) or $^{AV3}$KatE2 (lanes 5 and 6). (B) Catalase activity of cytosolic and periplasmic fractions (10 μg) from the indicated *E. coli* transformants. Control corresponds to the pKJE7 transformants without the pET derivatives. Each bar represents the average ± SD of three biological replicates (see table below) (C) Immunostaining of *E. coli* cytosolic-C or periplasmic-P fractions (15 μg) from pKJE7-transformed cells, cotransformed with pET22 vector (lanes 1 and 2), pEV3K2 (lanes 3 and 4), or pEV3K2$^{-P}$ (lanes 5 and 6). All data shown were obtained from four independent experiments.

*kat*$^-$ insertional mutant. This strain was used as host for the expression vectors pMV3K1 and pMV3K2 (Table 2) harboring the complete sequence of $^{AV3}$*katE1* and $^{AV3}$*katE2* genes, respectively, and including about 300 bp upstream from the ATG.

Tolerance of transformants to pro-oxidants was tested by placing serial dilutions drops of exponential cultures on agar plates supplemented with $H_2O_2$ or exposed to UV-B radiation immediately after plating. Results displayed in Fig. 6 show that, unlike $^{AV3}$KatE2, $^{AV3}$KatE1 was able to restore a tolerant phenotype similar to that observed for the *wt* ADP1 strain to pro-oxidant stressors, both $H_2O_2$ and UV radiation. Moreover, in the *kat*$^-$ transformants, the

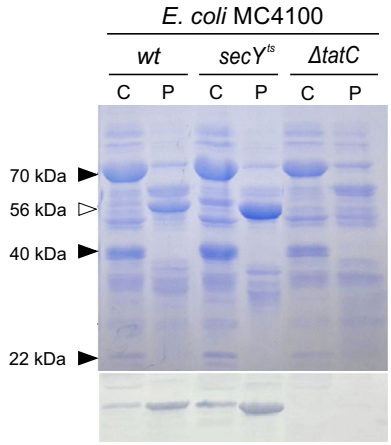


**Fig. 4.** Translocation of $^{AV3}$KatE2 to periplasm. Upper panel shows protein staining of SDS/PAGE of cytosolic-C or periplasmic-P fractions (15 μg) from *E. coli* MC4100-induced cells (*wt*), isogenic *secY*$^{ts}$ cells, or Δ*tatC* cotransformed with pKJE7 and pEV3K2. Black arrows indicate chaperone expression (70, 40, and 22 kDa); white arrow indicates $^{AV3}$KatE2 accumulation. Lower panel displays the immunostaining of the corresponding fractions detailed above employing anti-AV3KatE2 polyclonal antibodies. The figures displayed are representative of at least three biological replicates.

presence of $^{AV3}$KatE1 provided a higher tolerant phenotype in comparison with the contribution of $^{AVR}$-KatE2 (Fig. 6B). However, previous exposure of ADP1 *kat*$^{-}$ pMV3KE2 to low concentrations of $H_2O_2$ resulted in an increase of tolerance, suggesting a response of the $^{AVR}$*katE2* gene to peroxide (Fig 6B).

## Phylogenetic analysis of hydroperoxidases in the *Acinetobacter* genus

In order to explore the diversity of HP-encoding genes in the *Acinetobacter* genus, a local database including 114 publicly available complete genomes was constructed. It comprised 14 different *Acinetobacter* defined species plus 6 strains corresponding to unassigned species (Table S1). BLASTP-homology searches were then performed using as query the following proteins: $^{AV3}$KatE1 and $^{AV3}$KatE2 (EZQ12194.1 and EZQ11977.1, respectively), and *A. baumannii* ATCC17978 KatE-clade 2 and KatG (ABO11814.2 and ABO10867.2, respectively). Our comparative analysis showed a total of 302 putative catalases in the selected *Acinetobacter* strains.

A phylogenetic analysis including all these HPs, as well as those used as query, was then performed. It showed the presence of four well-supported clusters (Fig. 7). With this information, and following previous classifications [7,10,13], we were able to distinguish four groups:

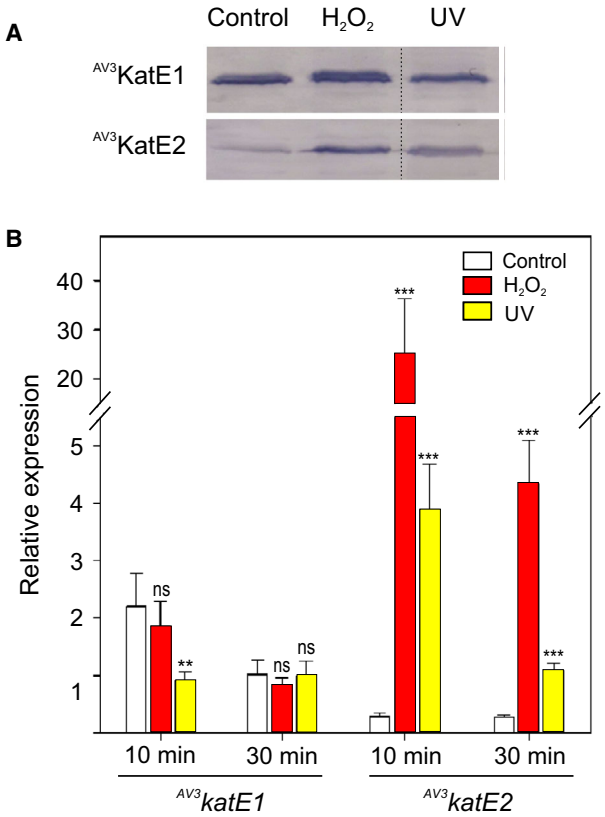


| | Control | $H_2O_2$ | UV |
|---|---|---|---|
| $^{AV3}$*katE1* (10 min) | 2.2 ± 0.6 | 1.8 ± 0.5 | 0.9 ± 0.2 |
| $^{AV3}$*katE1* (30 min) | 1.0 ± 0.2 | 0.8 ± 0.1 | 1.0 ± 0.2 |
| $^{AV3}$*katE2* (10 min) | 0.3 ± 0.1 | 25 ± 10 | 3.9 ± 0.8 |
| $^{AV3}$*katE2* (30 min) | 0.3 ± 0.1 | 4.3 ± 0.7 | 1.1 ± 0.1 |

**Fig. 5.** Expression of AV3katE1 and AV3katE2 after pro-oxidant challenges. (A) Immunostaining of total protein extracts (15 μg) employing anti-AV3KatE1 or anti-AV3KatE2 antibodies from untreated cells (control) or challenged with 1 mM $H_2O_2$ or 900 J·m$^{-2}$ UV exposure (four biological replicates data representation). The original gel had additional lanes that are not shown in the figure (indicated by a dotted line). (B) Expression of AV3katE1 or AV3katE2 relative to housekeeping genes (recA and rpoB mean) in untreated Ver3 cells (white bars), after 1 mM $H_2O_2$ challenge (red bars) or 900 J·m$^{-2}$ UV exposure (yellow bars). Asterisks indicate significant differences among control and treatments, as determined by analysis of variance (ANOVA) and Tukey's multiple comparison test. Each bar represents the average ± SD of four biological replicates (see table below).

i HPII or KatE, clade 1 contains 26 members. This is the less prevalent class in the analyzed strains. They are encoded by *A. baumannii* (18 strains), *A. equi*, *A. haemolyticus*, *A. lwoffii*, *A. schindleri*, and four strains not assigned to any validated species, including Ver3. All these proteins were

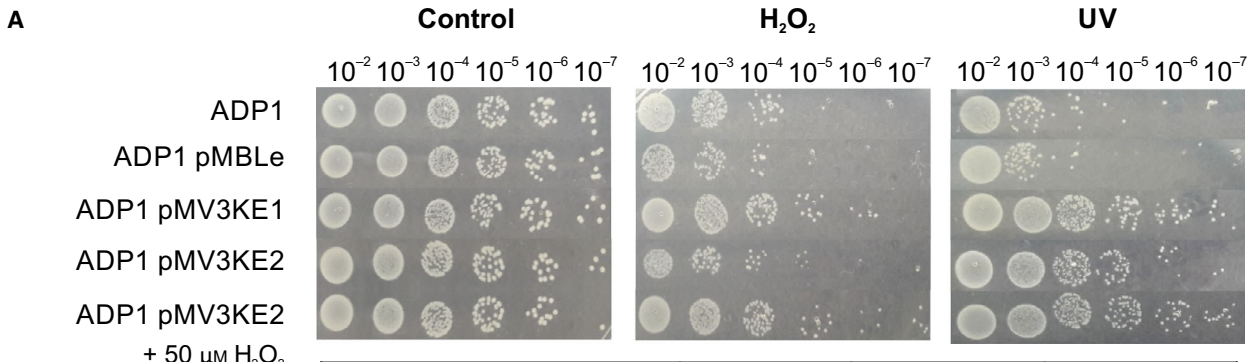


| | Control | $H_2O_2$ (250 μM) | UV (900 J·m$^{-2}$) |
|---|---|---|---|
| ADP1 | $1.6 \pm 0.4\ 10^7$ | $2.1 \pm 0.7\ 10^5$ | $2.9 \pm 0.4\ 10^5$ |
| ADP1 pMBLe | $2.5 \pm 0.6\ 10^7$ | $6.3 \pm 0.2\ 10^4$ | $9.0 \pm 0.3\ 10^4$ |
| ADP1 pMV3K1 | $1.2 \pm 0.2\ 10^7$ | $1.3 \pm 0.2\ 10^7$ | $1.2 \pm 0.3\ 10^7$ |
| ADP1 pMV3K2 | $1.1 \pm 0.2\ 10^7$ | $1.2 \pm 0.4\ 10^5$ | $2.8 \pm 0.1\ 10^6$ |
| ADP1 pMV3K2 +50 μM $H_2O_2$ | $3.2 \pm 0.6\ 10^7$ | $2.2 \pm 0.1\ 10^7$ | $1.6 \pm 0.3\ 10^7$ |

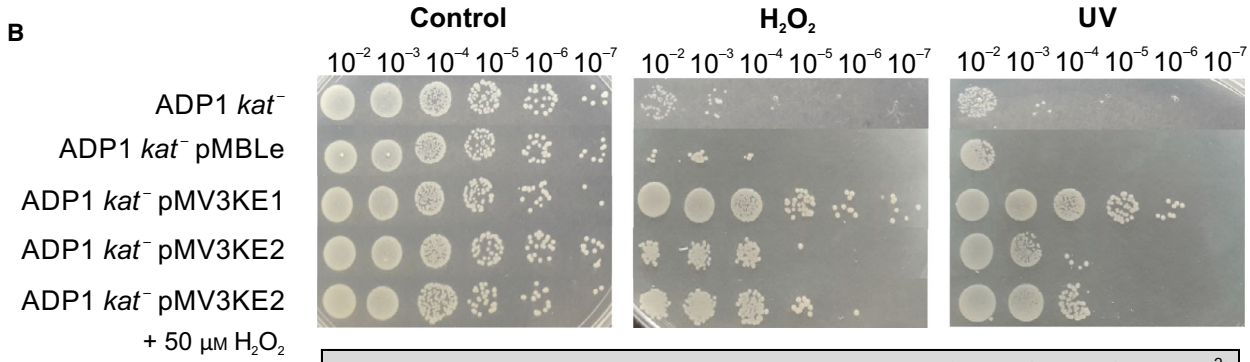


| | Control | $H_2O_2$ (100 μM) | UV (450 J·m$^{-2}$) |
|---|---|---|---|
| ADP1 *kat*$^-$ | $4.0 \pm 0.4\ 10^7$ | $5.0 \pm 0.3\ 10^5$ | $4.3 \pm 0.2\ 10^4$ |
| ADP1 *kat*$^-$pMBLe | $4.6 \pm 0.8\ 10^7$ | $1.6 \pm 0.6\ 10^6$ | $3.2 \pm 0.8\ 10^4$ |
| ADP1 *kat*$^-$pMV3K1 | $5.0 \pm 0.5\ 10^7$ | $1.6 \pm 0.3\ 10^7$ | $1.5 \pm 0.3\ 10^7$ |
| ADP1 *kat*$^-$pMV3K2 | $8.2 \pm 0.5\ 10^7$ | $4.7 \pm 0.3\ 10^5$ | $8.7 \pm 0.5\ 10^4$ |
| ADP1 *kat*$^-$pMV3K2 +50 μM $H_2O_2$ | $2.7 \pm 0.6\ 10^7$ | $8.3 \pm 0.4\ 10^6$ | $1.1 \pm 0.1\ 10^6$ |

**Fig. 6.** Effect of $^{AV3}$KatE1 and $^{AV3}$KatE2 on the tolerance of ADP1 wt (A) and *kat*$^-$ (B) to pro-oxidants. Aliquots (10 μL) of exponentially grown cultures ($OD_{600nm}$ 0.4) from parental, deficient, and complemented ADP1 derivative strains (indicated at left) were serially diluted and loaded onto LB agar plates supplemented with $H_2O_2$ or subjected to UV radiation. ADP1 wt and *kat*$^-$ complemented with pMV3K2 were additionally subjected to induction with 50 μM $H_2O_2$ for 30 min (bottom lane) prior to serial dilution. Tables indicate average colony-forming units counting (per mL) of three biological replicates.

predicted to encode a signal peptide and thus might be translocated to the periplasm as demonstrated herein for $^{AV3}$KatE2. With the exception of *Acinetobacter* sp. Ver3, TGL-Y2 and Ncu2D-2, strains encoding this type of catalase also harbor a gene coding for a HPI catalase–peroxidase.

ii HPII or KatE, clade 2 includes 104 members. These catalases were found in the 88 *A. baumannii* strains under study and in 16 out of 26 non-*baumannii*. We detected a group of five proteins present in non-*baumannii* *Acinetobacter* strains showing between 60% and 75% of identity to ABO11814.2 from *A. baumannii* ATCC17978. They might constitute a novel subclade within this group.

iii HPII or KatE, clade 3 is composed by 66 members (55 *A. baumannii* strains) showing > 84% of sequence identity to $^{AV3}$KatE1. Of note, the HPII

catalase encoded by *A. baylyi* ADP1 belongs to this group which also includes proteins encoded by seven non-*baumannii* and three strains not assigned to any validated species, such as Ver3.

iv HPI or KatG (catalase–peroxidase) has 106 members (87 *A. baumannii* strains) distributed among 14 out of the 16 *Acinetobacter* species under study, suggesting that they fulfill a critical role in the oxidative stress response. We additionally detected a group of 8 proteins present in non-*baumannii* *Acinetobacter* strains showing around 54% of identity to ABO10867.2 from *A. baumannii* ATCC 17978, which might constitute a novel clade (HPI-like) within this group.

## Discussion

High-altitude Andean lakes represent an important source of biological strategies to resist extreme environmental conditions. The isolates *Acinetobacter* sp. Ver3 and Ver7 have been shown to display enhanced resistance to pro-oxidant reagents such as $H_2O_2$ or MV. Moreover, a high tolerance to UV radiation was observed in both strains, and this feature seemed to be related to a high catalase activity present in the bacteria [4].

Analysis of the Ver3 genome sequence shows the presence of two catalase genes, CL42_01515 and CL42_02730 coding for two HPII named $^{AV3}$KatE1 and $^{AV3}$KatE2, respectively.

Cloning, recombinant expression and activity measurements of the protein products demonstrated that $^{AV3}$KatE1 is a heme catalase and corresponded to the main activity detected in Ver3 soluble extracts (Fig. 1C), displaying one of the highest rates described so far with a $k_{cat}$ of $1.3 \times 10^7$ $s^{-1}$ in many *Acinetobacter* species [14,15] and also other bacteria [16–18].

On the other hand, $^{AV3}$KatE2 is a HPII catalase with a putative N-terminal signal sequence. The construction of a vector without the signal peptide sequence enabled us to demonstrate that only the complete gene promotes expression of an active enzyme product, indicating that the N-terminal sequence is required for the proper folding of $^{AV3}$KatE2, subsequent catalytic activity, and correct transport to the periplasm (Fig. 2).

Localization of both catalases in *E. coli* cells was investigated by subcellular fractionation of the transformed bacteria. While $^{AV3}$KatE1 was found only in cytosolic fractions, $^{AV3}$KatE2 was directed to periplasm, as revealed by SDS/PAGE and activity measurements in soluble extracts (Fig. 3A,B). Moreover,

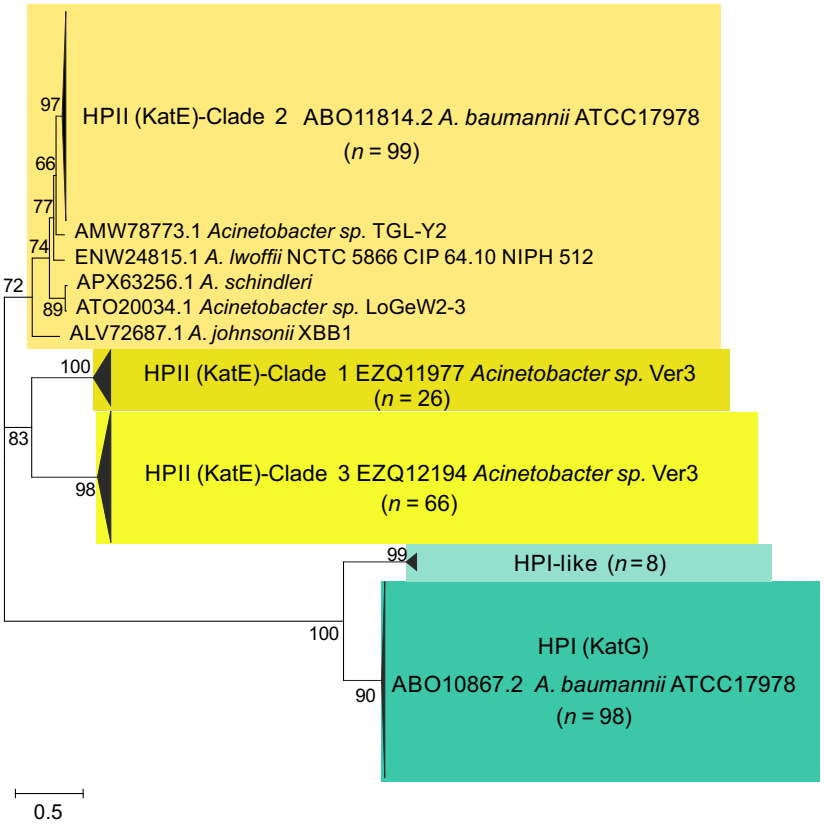


**Fig. 7.** Phylogenetic tree of catalases from *Acinetobacter* strains. The dendrogram was constructed with MEGA version 7.0 [37] using the NJ method, and the robustness of the major branching points is indicated by the bootstrap values (1000 repetitions).

the use of anti- $^{AV3}$KatE2 antibodies revealed that the enzyme lacking the signal peptide, encoded by the vector pEV3K2$^{-P}$, was notably less efficient in translocation (Fig. 3C).

In order to identify the mechanism of $^{AV3}$KatE2 targeting to the periplasm, the *E. coli secY*$^{ts}$ and Δ*tatC* mutants were used as host cells for the pEV3K2 vector. SDS/PAGE and subsequent immunostaining of subcellular fractions show that both the *wt* and *secY*$^{ts}$ strains accumulated the recombinant protein in the periplasm, while the Δ*tatC* strain did not, indicating that TAT was the translocation pathway used *in vivo* by the host cell to target $^{AV3}$KatE2 (Fig. 4). In contrast to the Sec pathway, the TAT system, present in *Archaea*, bacteria, and chloroplasts, facilitates the translocation of folded proteins across the lipid membrane bilayer from the cytosol to periplasm [19]. The lack of the TatC protein in the deficient host cell could be responsible of the complete absence of recombinant $^{AV3}$KatE2 in the cell after induction (Fig. 4), as TatC has been involved in substrate recognition, recruitment of the other protein components of the translocon, and stability of the whole complex [19,20].

It is worth noting, within this context, that the presence of homologues of both the SecY translocon and the TAT system proteins has been confirmed in *Acinetobacter* species through sequence comparison analysis (not shown).

The two AV3 catalases displayed contrasting responses to ROS propagators. While $^{AV3}$*kat*E1 transcripts failed to show significant changes in relative expression, $^{AV3}$*kat*E2 RNA levels rose about hundred times after 10 min of $H_2O_2$ treatment, and about twenty times following UV exposure. The increase in transcription was also reflected at the protein level as revealed by the use of specific antibodies (Fig. 5).

OxyR, PerR, and OhrR are the three best studied peroxide responsive regulators in bacteria [21], although only OxyR has been recently characterized in *A. baumannii* [22]. It was demonstrated in this bacterium that $H_2O_2$ presence triggers the oxidation of the OxyR C202 residue, leading to OxyR dissociation from the target *katE* gene promoter region and thus activating its transcription. The sequence alignment displayed in Fig. 8A shows the presence of the OxyR homologue found in *Acinetobacter* sp. Ver3 (*A.*Ver3 in the figure), including the conserved C202 involved in the activation of transcription previously described for *A. baumannii* [22], representing a likely candidate for the regulation of the transcriptional response of $^{AV3}$*kat*E2.

In order to identify a putative OxyR binding motif in the genes (*aphF1* and *aphF2* operons, *sul* genes, *katE*) whose transcription was reported to be modulated by this regulatory system in *A. baumannii* [22], the sequence of four promoters (−1 to −300) were extracted and analyzed using the MEME/MAST tool [23]. Three presumed sequence motifs were obtained by this method (not shown) which were subsequently employed as query for a search on the *katE1* and *katE2* promoter regions corresponding to *Acinetobacter* sp. Ver3. A putative candidate site was only found in the *katE2* promoter (CL42_02730; Fig. 8B), probably involved in the experimentally observed regulation of this gene (Fig. 5). Further experimental work would be needed to properly evaluate this hypothesis.

The influence of $^{AV3}$KatE1 and $^{AV3}$KatE2 on the tolerance of *A. baylyi* ADP1 *kat*$^{-}$ to $H_2O_2$ and UV radiation was evaluated using transformants grown on agar culture media plates. Results shown in Fig. 6 indicate that the cytosolic highly active $^{AV3}$KatE1 was able to restore *wt* levels of ROS tolerance to the mutants, with $^{AV3}$KatE2 being less efficient in conferring protection. However, a previous exposure of the pMV3K2 transformants to sublethal $H_2O_2$ concentrations promoted an increase in the tolerance of the host cell to pro-oxidants, suggesting a dose dependence of the protection capacity of the periplasmic $^{AV3}$KatE2 in ADP1 (Fig. 6).

A genomic comparative analysis of 114 *Acinetobacter* strains enabled to detect a great variability in the catalase classes harbored by this genus (Fig. 7 and Table 3). We observed that 99 strains, 81 corresponding to *A. baumannii*, harbor between 2 and 3 HPs, while 8 strains, 7 corresponding to *A. baumannii*, carry HP members belonging to the 4 established clusters. These results suggest that those *Acinetobacter* species usually associated with the clinical setting encode a higher number of HPs. In agreement with these observations, none of the 7 strains harboring only 1 HP is a representative of the *Acinetobacter baumannii-calcoaceticus* complex species. Moreover, the only catalase encoded in this group belong either to the clade 3 HPII group or the HPI novel subclade is observed in Fig. 7 (HPI-like), suggesting that the presence of at least one of these two HP classes is critical for survival in environmental *Acinetobacter* species.

Furthermore, the prevalence of the 4 HP classes in each strain was investigated and thus 10 different profiles were defined (Table 3). Following this classification, *Acinetobacter* sp. Ver3 presents a profile 2D (1 each HPII clades 1 and 3). Interestingly, only *Acinetobacter* sp. Ncu2D-2, a multisensitive strain isolated from the trachea of a mouse [24], shows an identical profile. We also detected that the profile 2A (1 each HPII clade 2 and HPI, see Table 3) encompasses the

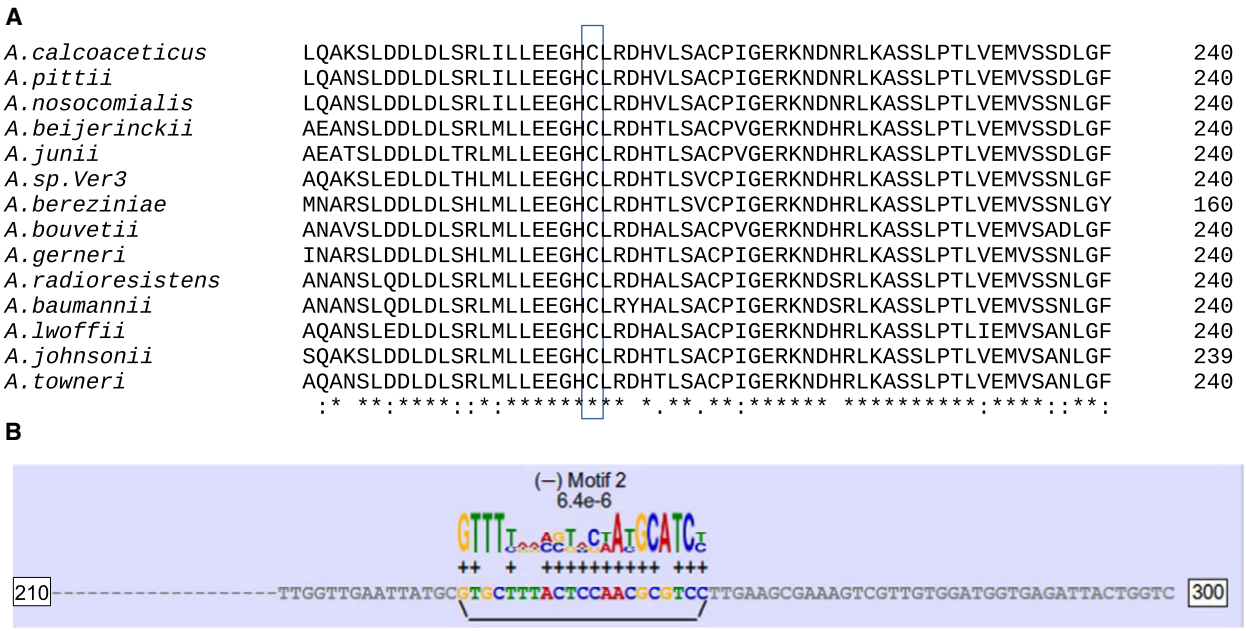


**Fig. 8.** *Acinetobacter* sp. Ver3 OxyR analysis (A) Alignment of OxyR sequences from representative members of the *Acinetobacter* genus, constructed with MUSCLE [36], implemented within MEGA version 7.0 [37]. Only the regions containing C202 are shown. *A. bereziniae* NIPH 3 (ENV22650.1), *A. gerneri* MTCC 9824 (EPR81597.1), *A. johnsonii* CIP 64.6 (ENU40121.1), *A. lwoffii* NIPH 478 (ENW30513.1), *A. towneri* DSM 14962 (WP_004972012.1), *A. radioresistens* DSM 6976 (ENV86475.1), *A. beijerinckii* CIP 110307 (ENW08376.1), *A. baumannii* 1239920 (WP_034681849.1), *A. junii* MTCC 11364 (EPR87172.1), *A. bouvetii* DSM 14964 (ENV83522.1), *A. calcoaceticus* NIPH 13 (ENU08372.1), *A. pittii* ANC 4050 (EOQ68101.1), *A. nosocomialis* (WP_016804061.1). (B) Putative OxyR binding site found in the *katE2* gene promoter of *Acinetobacter* sp. Ver3. Predictions were performed using MEME/MAST bioinformatic tools (see text for details).

highest diversity of *Acinetobacter* species, indicating this might be the most ubiquitous combination of HPs classes in this genus. Remarkably, the most prevalent profile among the strains under study is 3A (1 each HPII clades 2 and 3, and 1 HPI) with 50 occurrences (48 corresponding to *A. baumannii* strains). It is tempting to speculate that the expression of a HPII-clade 3 enzyme in this species provides an additional advantage during oxidative stress conditions.

The importance of catalases and peroxidases in ROS scavenging has been extensively studied. However, its involvement in the protection to radiation has recently attracted some attention. A pro-oxidant imbalance can be reached by an endogenous or exogenous increase of ROS formation and/or by a failure of the systems (including scavenging enzymes), but also by exposure to high-energy radiation [25]. Catalases are responsible for scavenging $H_2O_2$, the most important ROS involved in cysteine oxidation. Although classical models of radiation toxicity place DNA as preferred target, many bacteria are killed by radiation doses that cause little DNA injury, while protection of proteins from oxidative damage was claimed as an essential protective mechanism in radiation-resistant bacteria [26–28].

We presented here the first biochemical characterization of the catalases involved in the antioxidant response of the HAAL isolate *Acinetobacter* sp. Ver3 and demonstrated its contribution in the protection to UV radiation. On one hand, a catalytically efficient cytosolic enzyme is constitutively expressed in relatively high amounts protecting cytosol of pro-oxidant imbalance. On the other, an inducible isoenzyme, which is translocated to the periplasm via the TAT system, is responsible for preventing periplasmic protein peroxidation.

The number and type of different hydroperoxidases are also variable among *Acinetobacter* strains, with *A. baumannii* clinical isolates exhibiting higher numbers of isoenzymes and more variable profiles.

## Materials and methods

### Bacterial strains, plasmids, and culture media

Bacterial strains and plasmids used in this work are listed in Table 2. All strains were grown in Luria–Bertani (LB) broth, supplemented with 1.5% agar for solid medium when applicable. The antibiotics ampicillin (Ap) 100 $\mu g \cdot mL^{-1}$, kanamycin ($K_m$) 25 $\mu g \cdot mL^{-1}$, and chloramphenicol (Cm)

**Table 3.** Prevalence of HP classes in *Acinetobacter* strains under study.

| Organism | Occurrence | Clade 1 | Clade 2 | Clade 3 | HPI | Profile |
|---|---|---|---|---|---|---|
| *Acinetobacter baumannii* | 7 | 1 | 1 | 1 | 1 | 4 |
| *Acinetobacter schindleri* | 1 | 1 | 1 | 1 | 1 | |
| *Acinetobacter baumannii* | 48 | 0 | 1 | 1 | 1 | 3A |
| *Acinetobacter calcoaceticus* | 1 | 0 | 1 | 1 | 1 | |
| *Acinetobacter pittii* | 1 | 0 | 1 | 1 | 1 | |
| *Acinetobacter baumannii* | 10 | 1 | 1 | 0 | 1 | 3B |
| *Acinetobacter* sp. LoGeW2-3 | 1 | 1 | 1 | 0 | 1 | |
| *Acinetobacter* sp. TGL-Y2 | 1 | 1 | 1 | 1 | 0 | 3C |
| *Acinetobacter baumannii* | 22 | 0 | 1 | 0 | 1 | 2A |
| *Acinetobacter calcoaceticus* | 1 | 0 | 1 | 0 | 1 | |
| *Acinetobacter johnsonii* | 1 | 0 | 1 | 0 | 1 | |
| *Acinetobacter lactucae* | 1 | 0 | 1 | 0 | 1 | |
| *Acinetobacter nosocomialis* | 2 | 0 | 1 | 0 | 1 | |
| *Acinetobacter oleivorans* | 1 | 0 | 1 | 0 | 1 | |
| *Acinetobacter pittii* | 3 | 0 | 1 | 0 | 1 | |
| *Acinetobacter soli* | 1 | 0 | 1 | 0 | 1 | |
| *Acinetobacter* sp. DUT-2 | 1 | 0 | 1 | 0 | 1 | |
| *Acinetobacter equi* | 1 | 1 | 0 | 0 | 1 | 2B |
| *Acinetobacter haemolyticus* | 1 | 1 | 0 | 0 | 1 | |
| *Acinetobacter baumannii* | 1 | 1 | 1 | 0 | 0 | 2C |
| *Acinetobacter* sp. Ncu2D-2 | 1 | 1 | 0 | 1 | 0 | 2D |
| *Acinetobacter baylyi* ADP1 | 1 | 0 | 0 | 1 | 0 | 1A |
| *Acinetobacter bereziniae* | 1 | 0 | 0 | 1 | 0 | |
| *Acinetobacter junii* | 1 | 0 | 0 | 1 | 0 | |
| *Acinetobacter larvae* | 1 | 0 | 0 | 1 | 0 | |
| *Acinetobacter* sp. TTH0-4 | 1 | 0 | 0 | 1 | 0 | |
| *Acinetobacter haemolyticus* | 1 | 0 | 0 | 0 | 1 | 1B |
| *Acinetobacter junii* | 1 | 0 | 0 | 0 | 1 | |
| Total | | 26 | 104 | 66 | 106 | |

25 $\mu g \cdot mL^{-1}$ were added for selection as needed. *E. coli* strains were grown at 37 °C, unless otherwise indicated. *Acinetobacter* strains were grown at 30 °C.

## DNA manipulation procedures

*Acinetobacter* sp. Ver3 (AV3) and *A. baylyi* ADP1 genomic DNA were isolated following the CTAB method [29]. The $^{AV3}$*katE1* coding sequence was PCR-amplified using primers KatE1F and Kat1ER (Table 1). The amplification product was digested with *Nco*I and *Hind*III and ligated into the corresponding sites of the pET28 expression plasmid to generate pEV3K1. A similar procedure was performed for $^{AV3}$*katE*2 gene cloning with ($^{AV3}$*katE*2) and without ($^{AV3}$*katE2*$^{-p}$) its signal peptide sequence. Both sequences were PCR-amplified from Ver3 DNA using primers KatE2F and KatE2R or KatE2matF and KatE2R, respectively (Table 1). The amplification products were digested with *Nde*I and *Hind*III and cloned into the corresponding sites of pET22 to generate pEV3K2 and pEV3K2$^{-p}$.

The *A. baylyi* ADP1 *kat*$^{-}$-deficient strain was constructed by insertional mutation. The *katE* gene (ACIAD_RS02075, WP_004920274.1) was PCR-amplified from genomic DNA using KatEADPF and KatEADPR primers (Table 1). The 2332-bp product was cloned into pGEMT-Easy® to obtain pGAK1. A kanamycin cassette was then amplified by PCR from the pUC4K vector employing M13F and M13R primers (Table 1), and the generated product was cloned into pGAK1 at an EcoRV site to interrupt the *katE* gene, obtaining pGAK1km.

Plasmid pGAK1km was thus used as suicide vector to construct the ADP1 *kat*$^{-}$-deficient strain. Double recombination events were selected by loss of ampicillin resistance, and the mutants were checked by PCR and by loss of catalase activity as determined in a nondenaturing gel electrophoresis assay.

The pMV3K1 or pMV3K2 plasmids (Table 2) were used to complement ADP1 *kat*-deficient strain. $^{AV3}$*katE1* and $^{AV3}$*katE2* coding sequences including the ~ 300-bp upstream regulatory regions were PCR-amplified from Ver3 genomic DNA with primers KatE1up and KatE1R or KatE2up and KatE2R, respectively (Table 1). The resulting amplicons were digested with *Hind*III and ligated in the equivalent site of pMBLe(OA), generating pMV3K1 and pMV3K2.

All DNA digestions were performed following enzyme manufacturer's instructions. Constructions were verified by automated DNA sequencing.

## Protein expression and purification

The pEV3K1 plasmid was used to transform *E. coli* BL21 (DE3) pLysS, and purification of recombinant $^{AV3}$KatE1 was achieved as follows. Transformants were grown in LB broth supplemented with kanamycin and chloramphenicol at 37 °C to an $OD_{600nm}$ of 0.6. Expression of $^{AV3}$KatE1 was induced by incubation with 0.25 mM IPTG during 5 h at 180 r.p.m. Cells were harvested (4000 ***g*** at 4 °C, 15 min), resuspended in disruption buffer containing 50 mM Tris/HCl (pH 8), 0.1 mM EDTA, 50 mM NaCl, 0.5 mM phenylmethylsulfonyl fluoride protease inhibitor (PMSF), 0.5 mM $MgCl_2$, and 100 μg DNase per liter of culture, and lysed by sonication (Branson Sonifier 250, Branson Ultrasonics Corporation, Danbury, CT, USA). The suspension was cleared by centrifugation at 4 °C and 17 000 ***g*** for 30 min, and the supernatant was subjected to $(NH_4)_2SO_4$ precipitation at 30% (w/v) saturation. The precipitated proteins were collected by centrifugation (12 000 ***g*** at 4 °C, 15 min), the pellet was dissolved in 50 mM Tris (pH 8), and the suspension was dialyzed against 50 mM Tris/HCl (pH 8) and 50 mM NaCl. The solution was loaded onto a DEAE ion-exchange chromatography column equilibrated with 50 mM Tris/HCl (pH 8) and 50 mM NaCl. The enzyme was eluted with buffers of increasing ionic strength. The purified fraction containing $^{AV3}$KatE1 eluted at 200 mM NaCl.

*Escherichia coli* BL21 (DE3) cells harboring pKJE7 vectors (Takara®) encoding bacterial chaperones were used for the recombinant expression of $^{AV3}$KatE2 and $^{AV3}$KatE2$^{-p}$. Cells cotransformed with the pKJE7 derivatives and pEV3K2 or pEV3K2$^{-p}$ were cultured in LB broth supplemented with ampicillin and chloramphenicol. Arabinose (0.5 mg·mL$^{-1}$) was initially added to induce chaperone expression. Bacteria were grown at 37 °C until $OD_{600}$ reached 0.6, and then, the cells were preincubated for 30 min at 20 °C before the expression was induced with 0.5 mM IPTG during 16 h. Bacteria were pelleted, disrupted, and cleared as described above. The crude enzyme extract was precipitated by $(NH_4)_2SO_4$ 40% (w/v) saturation, the supernatant was removed, and the pellet was resuspended and dialyzed as described previously. The solution was loaded onto a DEAE ion-exchange chromatography column equilibrated with 50 mM Tris/HCl (pH 8) and 50 mM NaCl. The flow-through fractions, enriched in $^{AV3}$KatE2 or $^{AV3}$KatE2$^{-p}$, were pooled and loaded again onto a DEAE ion-exchange column. Fractions containing the recombinant catalases eluted with the flow-through at 50 mM NaCl in 50 mM Tris/HCl (pH 8).

*Escherichia coli* MC4100 wild-type (*wt*) and derivative strains (Table 2) were employed to identify the machinery utilized for $^{AV3}$KatE2 translocation. Cells cotransformed with pKJE7 and pEV3K2 were cultured in LB broth supplemented with ampicillin and chloramphenicol. Arabinose (0.5 mg·mL$^{-1}$) was initially added to induce chaperone expression. Bacteria were grown at 37 °C until $OD_{600}$ reached 0.6, and then, cells were preincubated for 30 min at 20 °C before the expression was induced with 0.5 mM IPTG during 16 h. Bacteria were pelleted, and the periplasmic-enriched fraction was isolated from the spheroplasts by subcellular fractionation.

## Subcellular fractionation

Subcellular fractionation was carried out in different pKJE7/*E. coli* cells co-expressing $^{AV3}$*katE1*, $^{AV3}$*katE2*, or $^{AV3}$*katE2*$^{-p}$. Briefly, 2–3 mL of cultures was pelleted (2000 ***g*** at 4 °C, 15 min), and cells were resuspended in 20 mM Tris/HCl (pH 8.5), 0.1 mM EDTA, 20% (w/v) sucrose, 1 mg·mL$^{-1}$ lysozyme, and 0.5 mM PMSF. Resuspension volume was normalized according to the formula $V = 0.05 \cdot OD_{600} \cdot V_c$, where $V_c$ was the starting volume of culture sample (in mL). The suspension was incubated at 4 °C for 30 min and finally pelleted (12 000 ***g*** at 4 °C, 15 min). The supernatant containing the periplasmic fraction was collected and stored on ice for further analysis. The pellet consisting of spheroplasts (i.e., the cytoplasmic fraction) was resuspended in the same volume of disruption buffer and was lysed by sonication as described above.

## Protein analysis

Protein concentration was determined by the Bradford method [30], using bovine serum albumin as standard. Protein purification steps and subcellular fractionations were followed by SDS/PAGE after Coomassie blue staining on a 12% (w/v) acrylamide gel according to the method of Laemmli [31].

Antibodies for $^{AV3}$KatE1 and $^{AV3}$KatE2 catalases were raised by the two consecutive injections of rabbits with 0.3 mg of purified proteins. The first subcutaneous injection was carried out with an emulsion 1 : 1 of the proteins with Freund's complete adjuvant (FCA). For second inoculations, Freund's incomplete adjuvant was employed instead of FCA.

For immunoblot analysis, proteins were transferred to nitrocellulose membranes. Alkaline phosphatase-conjugated goat anti-rabbit IgG was employed as secondary antibody (Sigma-Aldrich®, St. Louis, MI, USA). The antigen–antibody complex was detected by alkaline phosphatase reaction, employing 5-bromo-4-chloro-3-indolyl-phosphate (BCIP) and nitro blue tetrazolium (NBT) as substrates (Roche®, Roche Applied Sciences, Indianapolis, IN, USA).

### Spectroscopic measurements

Optical spectra were obtained at 25 °C in 50 mM Tris/HCl (pH 8) using a Cary WinUV UV-visible spectrophotometer equipped with a Cary Dual Cell Peltier accessory (Agilent Technologies, Santa Clara, CA, USA). Data were recorded every 0.5 nm between 200 and 800 nm.

### Catalase activity measurements

Catalase activity was measured spectrophotometrically by monitoring the decrease in absorbance at 240 nm resulting from the consumption of $H_2O_2$ using a Cary WinUV UV-visible spectrophotometer. The ε for $H_2O_2$ at 240 nm was 43.6 $M^{-1} \cdot cm^{-1}$ [32]. When indicated, catalase activity was also visualized *in situ* after electrophoresis in nondenaturing polyacrylamide gels as previously reported [33].

### RNA extraction and quantitative real-time reverse transcription PCR

Total RNA was isolated from *Acinetobacter* sp. Ver3 using TRI-Reagent® (Molecular Research Center, Inc., Cincinnati, OH, USA) according to the manufacturer's instructions. Quality and quantity of RNA were evaluated through agarose gel electrophoresis and spectrophotometry ($Abs_{260nm/280nm}$). Samples were treated with RQ1 RNase-free DNase (Promega, Madison, WI, USA) to remove possible DNA contamination prior to reverse transcription. To obtain cDNA, 2 μg of RNA was used in the RT reaction with random primers, employing M-MLV Reverse Transcriptase (Promega®), according to the manufacturer's instructions. Real-time PCRs were carried out on a StepOne device (Applied Biosystems, Thermo Fisher Scientific, Foster City, CA, USA) with 5× HOT FIREPol® EvaGreen® qPCR Mix Plus (ROX; Solis BioDyne, Tartu, Estonia) using specific primers (Table 1).

Results for $^{AV3}$*katE1* and $^{AV3}$*katE2* mRNAs were normalized to the *recA* and *rpoB* mRNA as housekeeping genes, based on the standard curve quantitative method [34]. The specificity of each reaction was verified by melting curves between 55 °C and 95 °C with continuous fluorescence measurements.

### Plate sensitivity assays

In order to evaluate tolerance to $H_2O_2$ or UV radiation, assays were performed as previously described [4]. Briefly, bacterial cultures were collected at 0.4 $OD_{600}$ nm and subjected to serial dilutions. Aliquots of 10 μL were then loaded onto LB agar plates, supplemented with $H_2O_2$, or exposed to 900 $J \cdot m^{-2}$ radiation using UVB lamps (BioRad, Richmond, CA, USA). The radiation intensity was measured using a UVB/UVA radiometer (UV203 AB radiometer; Macam Photometrics Ltd., Livingston, UK).

### Bioinformatics and comparative analysis

A comparative genomic analysis was performed that included all *Acinetobacter* strains available at the NCBI GenBank database. Only strains with a complete genome sequence were included in the analysis (Table S1). The genomic and proteomic data corresponding to 114 strains were extracted, and a local database was constructed. Catalases encoded by *Acinetobacter* sp. Ver3 and *A. baumannii* ATCC17978 were used as query to perform BLASTP-sequence similarity searches [35] against the local database, using 50% sequence identity and 70% query coverage cutoff values.

Using these data, phylogenetic trees were then constructed. A multiple alignment of the amino acid sequences of 302 inferred catalases was carried out using MUSCLE [36], implemented within the Molecular Evolutionary Genetics Analysis tool, MEGA version 7.0 [37]. This tool was also used to infer proteins phylogeny using the Neighbor-Joining method. Evolutionary distances were computed using the Poisson correction method [38]. Reliability of the inferred tree was tested by bootstrapping with 100 repetitions. SignalP 4.0 [39] and TMHMM Server v.2.0 (http://www.cbs.dtu.dk/services/TMHMM/) were used to predict signal peptides and transmembrane helices, respectively.

## Acknowledgements

The authors would like to acknowledge Virginia Perdomo for assistance with qRT-PCR measurements and Dr Néstor Carrillo for helpful discussions and for critically reading the manuscript. This work was supported by a grant from ANPCyT (PICT 2015-1492 to NC). MGS is a fellow of the CONICET, and GDR and NC are staff researchers of the same institution.

## Conflict of interest

The authors declare no conflict of interest.

## Author contributions

MGS designed and performed the experiments and participated in interpretation of the results. GDR accomplished the bioinformatics and sequence analysis. NC developed the conception and design of the work. All authors contributed to writing and editing the manuscript. This paper is dedicated to the memory of our dear colleague and friend, Dr Néstor Cortez, who passed away, while this paper was being peer-reviewed.

## References

1 Albarracín VH, Gärtner W & Farias ME (2016) Forged under the sun: life and art of extremophiles from Andean lakes. *Photochem Photobiol* **92**, 14–28.

2 Ordoñez OF, Flores MR, Dib JR, Paz A & Farías ME (2009) Extremophile culture collection from Andean lakes: extreme pristine environments that host a wide diversity of microorganisms with tolerance to UV radiation. *Microb Ecol* **58**, 461–473.
3 Flores MR, Ordoñez OF, Maldonado MJ and Farías ME (2009) Isolation of UV-B resistant bacteria from two high altitude Andean lakes (4,400 m) with saline and non saline conditions. *J Gen Appl Microbiol* **55**, 447–458.
4 Di Capua C, Bortolotti A, Farías ME & Cortez N (2011) UV-resistant *Acinetobacter* sp. isolates from Andean wetlands display high catalase activity. *FEMS Microbiol Lett* **317**, 181–189.
5 Albarracín VH, Pathak GP, Douki T, Cadet J, Borsarelli CD, Gärtner W & Farias ME (2012) Extremophilic acinetobacter strains from high-altitude lakes in Argentinean Puna: remarkable UV-B resistance and efficient DNA damage repair. *Orig Life Evol Biosph* **42**, 201–221.
6 Albarracín VH, Simon J, Pathak GP, Valle L, Douki T, Cadet J, Borsarelli CD, Farias ME & Gärtner W (2014) First characterisation of a CPD-class I photolyase from a UV-resistant extremophile isolated from High-Altitude Andean Lakes. *Photochem Photobiol Sci* **13**, 739–750.
7 Zámocký M, Gasselhuber B, Furtmüller PG & Obinger C (2012) Molecular evolution of hydrogen peroxide degrading enzymes. *Arch Biochem Biophys* **525**, 131–144.
8 Sun D, Crowell SA, Harding CM, De Silva PM, Harrison A, Fernando DM, Mason KM, Santana E, Loewen PC, Kumar A *et al.* (2016) KatG and KatE confer *Acinetobacter* resistance to hydrogen peroxide but sensitize bacteria to killing by phagocytic respiratory burst. *Life Sci* **148**, 31–40.
9 Kurth D, Belfiore C, Gorriti MF, Cortez N, Farias ME and Albarracín VH (2015) Genomic and proteomic evidences unravel the UV-resistome of the poly-extremophile *Acinetobacter* sp. Ver3. *Front Microbiol* **6**, 1–8.
10 Chelikani P, Fita I & Loewen PC (2004) Diversity of structures and properties among catalases. *Cell Mol Life Sci* **61**, 192–208.
11 Youn H-D, Yim Y-I, Kim K, Hah YC & Kang S-O (1995) Spectral characterization and chemical modification of catalase-peroxidase from *Streptomyces* sp. *J Biol Chem* **270**, 13740–13747.
12 Powers L, Hillar A & Loewen PC (2001) Active site structure of the catalase-peroxidases from *Mycobacterium tuberculosis* and *Escherichia coli* by extended X-ray absorption fine structure analysis. *Biochim Biophys Acta* **1546**, 44–54.
13 Klotz MG (2003) The molecular evolution of catalatic hydroperoxidases: evidence for multiple lateral transfer of genes between prokaryota and from bacteria into eukaryota. *Mol Biol Evol* **20**, 1098–1112.
14 Fu X, Wang W, Hao J, Zhu X & Sun M (2014) Purification and characterization of catalase from marine bacterium *Acinetobacter* sp. YS0810. *Biomed Res Int* **2014**, 1–7.
15 Muster N, Derecho I, Dallal F, Alvarez R, McCoy KB & Mogul R (2015) Purification, biochemical characterization, and implications of an alkali-tolerant catalase from the spacecraft-associated and oxidation-resistant *Acinetobacter gyllenbergii* 2P01AA. *Astrobiology* **15**, 291–300.
16 Lorentzen MS, Moe E, Jouve HM & Willassen NP (2006) Cold adapted features of Vibrio salmonicida catalase: characterisation and comparison to the mesophilic counterpart from *Proteus mirabilis*. *Extremophiles* **10**, 427–440.
17 Zeng H-W, Cai Y-J, Liao X-R, Zhang F & Zhang D-B (2011) Production, characterization, cloning and sequence analysis of a monofunctional catalase from *Serratia marcescens* SYBC08. *J Basic Microbiol* **51**, 205–214.
18 Sepasi Tehrani H & Moosavi-Movahedi AA (2018) Catalase and its mysteries. *Prog Biophys Mol Biol* **140**, 5–12.
19 Patel R, Smith SM & Robinson C (2014) Protein transport by the bacterial Tat pathway. *Biochim Biophys Acta* **1843**, 1620–1628.
20 Rollauer SE, Tarry MJ, Graham JE, Jääskeläinen M, Jäger F, Johnson S, Krehenbrink M, Liu S-M, Lukey MJ, Marcoux J *et al.* (2012) Structure of the TatC core of the twin-arginine protein transport system. *Nature* **492**, 210–214.
21 Dubbs JM & Mongkolsuk S (2016) Peroxide-sensing transcriptional regulators in bacteria. In Stress and Environmental Regulation of Gene Expression and Adaptation in Bacteria (de Bruijn FJ, ed), pp. 587–602. John Wiley & Sons Inc, Hoboken, NJ.
22 Juttukonda LJ, Green ER, Lonergan ZR, Heffern MC, Chang CJ & Skaar EP (2018) *Acinetobacter baumannii* OxyR regulates the transcriptional response to hydrogen peroxide. *Infect Immun* **87**, 413–418.
23 Bailey TL & Gribskov M (1998) Combining evidence using p-values: application to sequence homology searches. *Bioinformatics* **14**, 48–54.
24 Blaschke U & Wilharm G (2017) Complete genome sequence of *Acinetobacter* sp. strain NCu2D-2 isolated from a mouse. *Genome Announc* **5**, 415–416.
25 Davies MJ (2016) Protein oxidation and peroxidation. *Biochem J* **473**, 805–825.
26 Daly MJ, Gaidamakova EK, Matrosova VY, Vasilenko A, Zhai M, Leapman RD, Lai B, Ravel B, Li S-MW, Kemner KM *et al.* (2007) Protein oxidation implicated as the primary determinant of bacterial radioresistance. *PLoS Biol* **5**, e92.
27 Krisko A & Radman M (2010) Protein damage and death by radiation in *Escherichia coli* and *Deinococcus*

*radiodurans*. *Proc Natl Acad Sci USA* **107**, 14373–14377.
28 Krisko A & Radman M (2013) Phenotypic and genetic consequences of protein damage. *PLoS Genet* **9**, e1003810.
29 Sambrook J & Russell DW (2001) Molecular Cloning: A Laboratory Manual, 3rd edn. Cold Spring Harbor Laboratory, New York, NY.
30 Bradford MM (1976) A rapid and sensitive method for the quantitation of microgram quantities of protein utilizing the principle of protein-dye binding. *Anal Biochem* **72**, 248–254.
31 Laemmli UK (1970) Cleavage of structural proteins during the assembly of the head of bacteriophage T4. *Nature* **227**, 680–685.
32 Hildebrandt AG & Roots I (1975) Reduced nicotinamide adenine dinucleotide phosphate (NADPH)-dependent formation and breakdown of hydrogen peroxide during mixed function oxidation reactions in liver microsomes. *Arch Biochem Biophys* **171**, 385–397.
33 Scandalios JG (1968) Genetic control of multiple molecular forms of catalase in maize. *Ann N Y Acad Sci* **151**, 274–293.
34 Pfaffl MW & Hageleit M (2001) Validities of mRNA quantification using recombinant RNA and recombinant. *Biotechnol Lett* **23**, 275–282.
35 Altschul SF, Gish W, Miller W, Myers EW & Lipman DJ (1990) Basic local alignment search tool. *J Mol Biol* **215**, 403–410.
36 Edgar RC (2004) MUSCLE: multiple sequence alignment with high accuracy and high throughput. *Nucleic Acids Res* **32**, 1792–1797.
37 Kumar S, Stecher G & Tamura K (2016) MEGA7: molecular evolutionary genetics analysis version 7.0 for bigger datasets. *Mol Biol Evol* **33**, 1870–1874.
38 Zuckerkandl E & Pauling L (1965) Evolutionary divergence and convergence in proteins. In Evolving Genes and Proteins (Bryson V & Vogel HJ, eds), pp. 97–166. Elsevier, Amsterdam.
39 Petersen TN, Brunak S, von Heijne G & Nielsen H (2011) SignalP 4.0: discriminating signal peptides from transmembrane regions. *Nat Methods* **8**, 785.
40 Woodcock DM, Crowther PJ, Doherty J, Jefferson S, DeCruz E, Noyer-Weidner M, Smith SS, Michael MZ & Graham MW (1989) Quantitative evaluation of *Escherichia coli* host strains for tolerance to cytosine methylation in plasmid and phage recombinants. *Nucleic Acids Res* **17**, 3469–3478.
41 Studier FW & Moffatt BA (1986) Use of bacteriophage T7 RNA polymerase to direct selective high-level expression of cloned genes. *J Mol Biol* **189**, 113–130.
42 Casadaban MJ & Cohen SN (1980) Analysis of gene control signals by DNA fusion and cloning in *Escherichia coli*. *J Mol Biol* **138**, 179–207.
43 Baba T, Jacq A, Brickman E, Beckwith J, Taura T, Ueguchi C, Akiyama Y & Ito K (1990) Characterization of cold-sensitive secY mutants of *Escherichia coli*. *J Bacteriol* **172**, 7005–7010.
44 Bogsch EG, Sargent F, Stanley NR, Berks BC, Robinson C & Palmer T (1998) An essential component of a novel bacterial protein export system with homologues in plastids and mitochondria. *J Biol Chem* **273**, 18003–18006.
45 Taylor LA & Rose RE (1988) A correction in the nucleotide sequence of the Tn903 kanamycin resistance determinant in pUC4K. *Nucleic Acids Res* **16**, 7762–7762.
46 González LJ, Bahr G, Nakashige TG, Nolan EM, Bonomo RA & Vila AJ (2016) Membrane anchoring stabilizes and favors secretion of New Delhi metallo-β-lactamase. *Nat Chem Biol* **12**, 516–522.

## Supporting information

Additional supporting information may be found online in the Supporting Information section at the end of the article.

**Table S1.** Strains used for the bioinformatic analysis.